

---

# Modeling trend in temperature volatility using generalized LASSO

---

Anonymous Author(s)

Affiliation

Address

email

## Abstract

1 words, words,

## 2 1 Introduction

3 **TODO: Arash: Some equations do not have numbering and some have.**

4 **TODO: Arash: fix appendicies and the references to them.**

5 Nonparametric variance estimation for spatio-temporal data.

### 6 1.1 Motivating applications

7 **TODO: cut this down**

8 There is a considerable interest in determining if there is an increasing trend in the climate variability  
9 [8, 10]. An increase in the temperature variability will increase the probability of extreme hot outliers.  
10 It might be harder for the society to adapt to these extremes than to the gradual increase in the mean  
11 temperature [10].

12 In this paper, we consider the problem of detecting the trend in the temperature volatility. All analyses  
13 are performed on a sub-set of the European Centre for Medium-Range Weather Forecasts (ECMWF)  
14 ERA-20C dataset [26]. This dataset include the temperature measurements over a grid over the earth  
15 from 1957 to 2002. [6, 18, 19, 25, 27]

16 Research on analyzing the trend in the volatility of spatio-temporal data is scarce. [8] studied the  
17 change in the standard deviation (SD) of the surface temperature in the NASA Goddard Institute  
18 for Space Studies gridded temperature data set. In their analysis, for each geographical position,  
19 the mean of the temperature computed for the period 1951-1980 (called the base-period) at that  
20 position, is subtracted from the corresponding time series. Each time series is then divided by the  
21 standard deviation computed at each position and during the same time period. The distribution of  
22 the resulting data is then plotted for different periods. These distributions represent the deviation  
23 of the temperature for a specific period, from the mean in the base period, in units of the standard  
24 deviation in that period. The results showed that these distributions are wider for the recent time  
25 periods compared to 1951-1980. [10] took a similar approach in analysing the ERA-40 data set.  
26 However, in addition to the aforementioned method, they computed the distribution of the SDs in  
27 an alternative way: for each position and each time period, the deviation of the time-series at that  
28 position from the mean in that time period at that position was computed, and then divided by the SD  
29 of that position in the period before 1981. The results showed that there still is an increase in the SDs  
30 from 1958-1970 to 1991-2001, but this is much less than what is obtained from the method used in  
31 [8]. The authors also computed the time-evolving global SD from the de-trended time-series at each  
32 position. The resulting curve suggested that the global SD has been stable.

These previous work (and other related research, e.g., [16]) have several shortcomings. First, no statistical analysis has been performed to examine if the change in the SD is statistically significant. Second, the methodologies for computing the SDs are rather arbitrary. The deviation of each time-series in a given period, is computed from either the mean of a base-period (as in [8]), or from the given period (as in [10, 16]). These deviations are then normalized using the SD of the base-period or the given period. No justification is provided for these choices. Third, the correlation between the observations is ignored. The observations in subsequent days and close geographical positions could be highly correlated. Without considering these correlations, any conclusion based on the averaged data could be flawed.

The main contribution of this work is to develop a new methodology for detecting the trend in the volatility of spatio-temporal data. In this methodology, the variance at each position and time, is considered as a hidden (un-observed) variable. The value of these hidden variables are then estimated by maximizing the likelihood of the observed data. We show that this formulation per se, is not appropriate for detecting the trend. To overcome this issue, we penalize the differences between the estimated variances of the observations which are temporally and/or spatially close to each other. This will result in an optimization problem called the *generalized LASSO problem* [21]. As we will see, the dimension of this optimization problem is very high and so the standard methods for solving the generalized LASSO cannot be applied directly. We investigate two methods for solving this optimization problem. In the first method, we adopt an optimization technique called alternative direction method of multipliers (ADMM) [4], to divide the total problem into several sub-problems of much lower dimension and show how the total problem can be solved by iteratively solving these sub-problems. The second method, called the *linearized ADMM algorithm* [14] solves the main problem by iteratively solving a linearized version of it. We will compare the benefits of each method.

Also neuroscience.

## 1.2 Related work

Mention [7, 12]. Also, [22, 23]. ARCH/GARCH. [13, 17, 28] [15]

## 1.3 Main contributions

- We propose a model for non-parametric variance estimation for a spatio-temporal process ( Section 2).
- We derive two algorithms to fit our estimator when applied to very large data ( Section 3).
- We illustrate our methods on a large global temperature dataset with the goal of tracking world-wide trends in variance as well as a simulation constructed to mimic these data's features ( Section 4).

## 2 $\ell_1$ -trend filtering for estimating variance of a time-series

**TODO: Arash: shouldn't the title of this section be "...estimating variance of spatio-temporal data" or something similar?**

$\ell_1$ -trend filtering was proposed by [11] as a method for estimating a smooth, time-varying trend. It is formulated as the optimization problem

$$\min_{\beta} \frac{1}{2} \sum_{t=1}^T (y_t - \beta_t)^2 + \lambda \sum_{t=1}^{T-2} |\beta_t - 2\beta_{t+1} + \beta_{t+2}|$$

or equivalently:

$$\min_{\beta} \frac{1}{2} \|y - \beta\|_2^2 + \lambda \|D\beta\|_1 \quad (1)$$

where  $y_t$  is an observed time-series,  $\beta$  is the smooth trend,  $D$  is a  $(T - 2) \times T$  matrix, and  $\lambda$  is a tuning parameter which balances fidelity to the data (small errors in the first term) with a desire for smoothness. With the penalty matrix  $D$ , the estimated  $\beta$  will be piecewise linear. [11] proposed a specialized primal-dual interior point (PDIP) algorithm for solving (1). From a statistical perspective,

(1) is a constrained maximum likelihood problem with independent observations from a normal distribution with common variance,  $y_t \sim \mathcal{N}(\beta_t, \sigma^2)$ , subject to a piecewise linear constraint on  $\beta$ .

## 2.1 Estimating the variance

Inspired by the  $\ell_1$ -trend filtering algorithm, we propose a non-parametric model for estimating the variance of a time-series. To this end, we assume that at each time step  $t$ , there is a hidden variable  $h_t$  such that conditioned on  $h_t$  the observations  $y_t$  are independent normal variables with zero mean and variance  $\exp(h_t)$ . The negative log-likelihood of the observed data in this model is  $l(y | h) \propto -\sum_{t=1}^T h_t - y_t^2 e^{-h_t}$ . Crucially, we assume that the hidden variables  $h_t$  vary smoothly. To impose this assumption, we estimate  $h_t$  by solving the penalized, negative log-likelihood:

$$\min_h -l(y | h) + \lambda \|Dh\|_1 \quad (2)$$

where  $D$  has the same structure as above.

**TODO: explain the objective more. give the AR(1) example. Explain what you loses by this assumption (ACF, forecasting). Also explain that the covariace matrix is diagonal so it cannot capture the covariance structure. But in contrast to spatial stat literature, it does not make any assumption on estimated variances. Compare to Hallac et al and Lingren et al.**

As with (1), one can solve (2) using the PDIP algorithm (as in, e.g., cvxopt [1]). In each iteration of PDIP we need to compute a *search direction* by taking a Newton step on a system of nonlinear equations. Appendix B provides details on how this computation can be performed for the objective function 2.

**TODO: Arash: I think we should remove Algorithm 1. There are other steps in PDIP which involve adapting the algorithm parameter  $w$  and doing Backtracking line search. Also there is only one loop in PDIP.**

## 2.2 Adding spatial constraints

The method in the previous section can be used to estimate the variance of a single time-series. In this section, we extend this method to the estimation of the variance of spatio-temporal data.

At a specific time  $t$ , the data is measured on a grid of points with  $n_r$  rows and  $n_c$  columns for a total of  $S = n_r \times n_c$  spatial locations. Let  $y_{ijt}$  denote the value of the observation at time  $t$  on the  $i^{\text{th}}$  row and  $j^{\text{th}}$  column of the grid, and  $h_{ijt}$  denote the corresponding hidden variable. We seek to impose both temporal and spatial smoothness constraints on the hidden variables. Specifically, we seek a solution for  $h$  which is piecewise linear in time and piecewise constant in space (although higher-order smoothness can be imposed with minimal alterations to the methodology). We achieve this goal by solving the following optimization problem:

$$\begin{aligned} \min_h \sum_{i,j,t} h_{ijt} + y_{ijt}^2 e^{-h_{ijt}} + \lambda_1 \sum_{i,j} \sum_{t=1}^{T-2} |h_{ijt} - 2h_{ij(t+1)} + h_{ij(t+2)}| \\ + \lambda_2 \sum_{t,j} \sum_{i=1}^{n_r-1} |h_{ijt} - h_{(i+1)jt}| + \lambda_2 \sum_{t,i} \sum_{j=1}^{n_c-1} |h_{ijt} - h_{i(j+1)t}| \end{aligned} \quad (3)$$

The first term in the objective is proportional to the negative log-likelihood, the second is the temporal penalty for the time-series at each location  $(i, j)$ , while the third and fourth, penalize the difference between the estimated variance of two vertically and horizontally adjacent points, respectively. The spatial component of this penalty is a special case of trend filtering on graphs [29] which penalizes the difference between the estimated values of the signal on the connected nodes. As before, we can write (3) in matrix form where  $h$  is an  $T \times S$  vector and  $D$  is replaced by  $D_{TS} \in \mathbb{R}^{(N_t+N_s) \times (T \cdot S)}$ , where  $N_t = S \cdot (T - 2)$  and  $N_s = T \cdot (2n_r n_c - n_r)$  are the number of temporal and spatial constraints, respectively<sup>1</sup>. Then, as we have two different tuning parameters for the temporal and

<sup>1</sup> $N_s$  is obtained by counting the number of unique constraints at each location and at all times.

116 spatial components, we write  $\Lambda = [\lambda_1 \mathbf{1}_{N_t}^\top, \lambda_2 \mathbf{1}_{N_s}^\top]^\top$  leading to <sup>2</sup>:

$$\min_h -l(y | h) + \Lambda^\top |D_{TS}h| \quad (4)$$

117 **TODO: Add back the full form of  $D$  above? It was too cumbersome before, but possibly necessary**

### 118 3 Proposed optimization methods

119 For a spatial grid of size  $S$  and  $T$  time steps,  $D_{ST}$  will have  $3Tn_r n_c - 2n_r n_c - Tn_r$  rows and  $ST$   
 120 columns. For a  $1^\circ \times 1^\circ$  grid over the entire northern hemisphere and daily data over 10 years, we  
 121 have  $n_r = 90$ ,  $n_c = 180$ ,  $T = 3650$  and so  $D_{ST}$  has approximately  $10^8$  columns and  $10^8$  rows. In  
 122 each step of the PDIP algorithm, we need to solve a linear system of equations in  $A$  which depends  
 123 on  $D_{ST}^\top D_{ST}$  (see appendix A and B). Therefore, applying the PDIP directly is infeasible for our  
 124 data.<sup>3</sup>

125 In the next section, we develop two ADMM algorithms for solving this problem efficiently. The  
 126 first casts the problem as a so-called consensus optimization problem [4] which solves smaller  
 127 sub-problems using PDIP and then recombines the results. The second uses proximal methods to  
 128 avoid matrix inversions.

129 **TODO: We note that stochastic gradient descent could be used but...**

130 **TODO: Arash: The primal objective is not differentiable and so we cannot use SGD. The dual has**  
 131 **constraints and so the plane SGD cannot be used. We can use projected SGD but I think it would**  
 132 **converge slowly. Since other papers on LASSO have not considered SGD I don't think we need to**  
 133 **justify why we did not use it.**

#### 134 3.1 Consensus optimization

135 Consider an optimization problem of the form  $\min_h f(h)$ , where  $h \in \mathbb{R}^n$  is the *global variable* and  
 136  $f(h) : \mathbb{R}^n \rightarrow \mathbb{R} \cup \{+\infty\}$  is convex. The goal in consensus optimization is to break this problem into  
 137 several smaller sub-problems which can be solved independently in each iteration of optimization.

138 Assume that it is possible to define a set of *local variables*  $x_i \in \mathbb{R}^{n_i}$  such that  $f(h) = \sum_i f_i(x_i)$ ,  
 139 where each  $x_i$  is a subset of the global variable  $h$ . More specifically, each entry of the local variables  
 140 corresponds to an entry of the global variable. Therefore we can define a mapping  $\mathcal{G}(i, j)$  from the  
 141 local variables indices into the global variable indices:  $k = \mathcal{G}(i, j)$  means that the  $j^{\text{th}}$  entry of  $x_i$   
 142 is  $h_k$  (or  $(x_i)_j = h_k$ ). For ease of notation, define  $\tilde{h}_i \in \mathbb{R}^{n_i}$  as  $(\tilde{h}_i)_j = h_{\mathcal{G}(i, j)}$ . Then, the original  
 143 optimization problem is equivalent to the following problem:

$$\begin{aligned} \min_{\{x_1, \dots, x_N\}} \quad & \sum_i f_i(x_i) \\ \text{s.t.} \quad & \tilde{h}_i = x_i \end{aligned}$$

144 It is important to note that each entry of the global variable may correspond to several entries of  
 145 the local variables and so the constraints  $\tilde{h}_i = x_i$  enforce the consensus between the local variables  
 146 corresponding to the same global variable.

147 The *augmented Lagrangian* corresponding to the problem 3.1 is  $L_\rho(x, h, y) = \sum_i (f_i(x_i) + u_i^\top (x_i -$   
 148  $\tilde{h}_i) + (\rho/2) \|x_i - \tilde{h}_i\|_2^2)$ . Now, we can apply ADMM to  $L_\rho$  which results in the following ADMM  
 149 updating steps at each iteration  $m$ :

<sup>2</sup>Throughout the paper, we use  $|x|$  for both scalars and vectors. For vectors we use this to denote a vector obtained by taking the absolute value of each entry of  $x$ .

<sup>3</sup>We note that this is a highly structured and sparse matrix, but, unlike trend filtering alone, it is not banded. We are unaware of general linear algebra techniques for inverting such matrix, despite our best efforts.

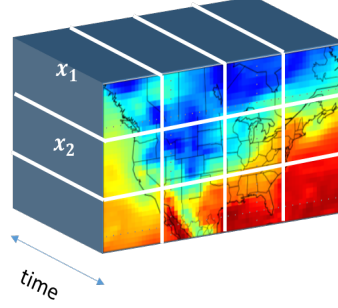


Figure 1: The cube represents the global variable  $h$  in space and time. The sub-cubes specified by the white lines are  $x_i$ . **TODO: Can we use  $h_i$  here instead of  $x_i$ ?**

$$\begin{aligned}
 x_i^{m+1} &:= \underset{x_i}{\operatorname{argmin}} \left( f_i(x_i) + (u_i^m)^\top x_i + (\rho/2) \|x_i - \tilde{h}_i^m\|_2^2 \right) \\
 h_k^{m+1} &:= (1/S_k) \sum_{\mathcal{G}(i,j)=k} (x_i^{m+1})_j \\
 u_i^{m+1} &:= u_i^m + \rho(x_i^{m+1} - \tilde{h}_i^{m+1})
 \end{aligned} \tag{5}$$

150 Here,  $S_k$  is the number of local variable entries that correspond to  $h_k$ , and  $u_i$  are the Lagrange  
 151 multipliers.

152 **TODO: I don't much like this explanation or notation. Seems unclear**

153 **TODO: Arash: I re-wrote this section.**

154 To solve the optimization problem (4) or (3) using this method, we need to address two questions:  
 155 first, how to choose the local variables  $x_i$ , and second, how to solve the optimization problem for  
 156 updating these variables (the first line of (5) which we will refer to it as *x-update step*).

157 In 1, the global variable  $h$  is represented as a cube (using the subset of the US as an example). We  
 158 decompose  $h$  into sub-cubes as shown in the figure by white lines. It is easy to see that by this  
 159 definition of  $x_i$ , the objective (4) decomposes as  $\sum_i f_i(x_i)$  where  $f_i(x_i) = -l(y_i | x_i) + \Lambda_{(i)}^\top |D_{(i)} x_i|$ ,  
 160 and  $\Lambda_{(i)}$  and  $D_{(i)}$  contain the temporal and spatial penalties corresponding to  $x_i$  only. The x-update  
 161 step in Equation 5 is the following optimization problem:  $x_i^{m+1} := \underset{x_i}{\operatorname{argmin}} (f_i(x_i) + (u_i^m)^\top x_i +$   
 162  $(\rho/2) \|x_i - \tilde{z}_i^m\|_2^2)$ .

163 **TODO: I would like to be able to write all this in terms of  $h$  instead of  $x$**

164 **TODO: Arash: now I'm using  $h$  as the global variables. We cannot write the local variables in terms**  
 165 **of  $h$  since they are different from  $h$ .**

166 By this definition of  $x_i$ , the update step for  $x_i$  is the following optimization problem:  $x_i^{m+1} :=$   
 167  $\underset{x_i}{\operatorname{argmin}} (f_i(x_i) + (u_i^m)^\top x_i + (\rho/2) \|x_i - \tilde{z}_i^m\|_2^2)$ . We solve this using the PDIP method. As it was  
 168 explained in Section 2.1, to use PDIP we need to compute the dual problem, which in turn needs the  
 169 computation of the Fenchel conjugate of the loss function. In addition, referring to ??, we need to  
 170 compute the gradient and Jacobian of the conjugate functions. It is important to note that compare to  
 171 the optimization problem Equation 2, the loss function in the x-update step in Equation 5 includes the  
 172 quadratic term  $(\rho/2) \|x_i - \tilde{z}_i^m\|_2^2$ . This makes the computation more involved than Section 2.1. The  
 173 details of the computations are explained in Section 7. **TODO: change this to appendix**

174 **TODO: I'm not sure if we want to devote some space to write this as a separate algorithm. The steps**  
 175 **are those mentioned in 5 and the x-update is now explained in the appendix. So we may want to**  
 176 **remove algorithm 1.**

177 The complete ADMM algorithm for estimating the variances is represented in Algorithm 1. All the  
 178 computations in the three updating steps (5) can be performed in parallel. The number of rows and

---

**Algorithm 1** ADMM for sparse estimation of variance of spatio-temporal data TODO: Fix this


---

**Input:** data  $y$ , mapping  $\mathcal{G}(i, j)$ ,  $\rho$ ,  $\lambda_t$ ,  $\lambda_s$   
 Initialization:  $x_i^0 = z^0 = u_i^0 = \mathbf{0}$ .  
**for**  $m = 1, 2, \dots$  **do**  
   **for**  $i = 1$  **to**  $N_{sub-cubes}$  **do**  
     compute  $\nu_i$  from (??)  
     compute  $w_i$  from (??)  
     set  $x_i^m := w_i$   
   **end for**  
   Compute  $z^m$  from (5)  
   Compute  $u_i^m$  from (5)  
**end for**

---

179 columns of the sub-cubes should be chosen so that the updating of  $x_i$  could be performed in one  
 180 processor. We choose  $3 \times 3 \times 521$  sub-cubes.

181 Because Algorithm 1 breaks the large optimization into sub-problems that can be solved independently,  
 182 it is amenable to a split-gather parallelization strategy via, e.g., the map reduce framework. In each  
 183 iteration, the computation time will be equal to the time to solve each sub-problem plus the time  
 184 to communicate the solutions on the master processor and perform the consensus step. Since each  
 185 sub-problem is small, with parallelization, the computation time in each iteration will be small. In  
 186 addition, our experiments with several values of  $\lambda_t$  and  $\lambda_s$  showed that the algorithm converges in  
 187 few hundreds iterations. TODO: Need to redo this: Solving each sub-problem on a machine with  
 188 four 3.20GHz Intel i5-3470 cores takes less than 3 seconds on average, and so for example if we  
 189 assume that communication time is 10 seconds and the algorithm converges in 300 iterations, with  
 190 parallelization on  $N_{sub-cubes}$  machines, the algorithm will converge in about 1 hour. Assuming that  
 191 we use  $N_{sub-cubes}$  machines and that the convergence rate of the algorithm is independent of the  
 192 grid size, this time will be independent of the grid size.

193 If we perform these computations on a single machine, the computation time grows linearly with  
 194  $N_{sub-cubes}$ . For example, for the data in a grid over the united states and using  $3 \times 3 \times 521$  sub-cubes  
 195 each iteration of the algorithm will take about 20 minutes on a single machine and so with 300  
 196 iterations it will take several days to converge. Given that we need to compute the solution for several  
 197 values of the parameters  $\lambda_t$  and  $\lambda_s$ , this computation time is not feasible.

198 Therefore, this algorithm is only useful if we can parallelize the computation over several machines.  
 199 In the next section, we describe another algorithm which makes the computation feasible on a single  
 200 machine.

### 201 3.2 Linearized ADMM

202 TODO: Need a good dummy variable here, it can't be  $u$ . Consider the generic optimization problem  
 203  $\min_x f(x) + g(Dx)$  where  $x \in \mathbb{R}^n$  and  $D \in \mathbb{R}^{m \times n}$ . Each iteration of the linearized ADMM  
 204 algorithm [14] for solving this problem has the form

$$\begin{aligned}
 x &\leftarrow \underset{\mu f}{\text{prox}} \left( x - (\mu/\rho) D^\top (Dx - z + u) \right) \\
 z &\leftarrow \underset{\rho g}{\text{prox}} (z + u) \\
 u &\leftarrow u + Dx - z
 \end{aligned} \tag{6}$$

205 where the algorithm parameters  $\mu$  and  $\rho$  satisfy  $0 < \mu < \rho / \|D\|_2^2$ ,  $z, u \in \mathbb{R}^m$  and the proximal  
 206 operator is defined as

$$\underset{\alpha f}{\text{prox}}(u) = \min_x \alpha \cdot f(x) + \frac{1}{2} \|x - u\|_2^2.$$

207 TODO: What are  $\mu$  and  $\rho$ ?

---

**Algorithm 2** Linearized ADMM

---

**Input:** data  $y$ , penalty matrix  $D$ ,  $\rho, \lambda_t, \lambda_s > 0$ .

**Set:**  $h \leftarrow 0, z \leftarrow 0, u \leftarrow 0$ .

**for**  $m = 1, 2, \dots$  **do**

$$h_k \leftarrow \mathcal{W}\left(\frac{y_k^2}{\mu} \exp\left(\frac{1-\mu u_k}{\mu}\right)\right) + \frac{1-\mu u_k}{\mu},$$

$$z \leftarrow S_{\rho\lambda}(u).$$

$$u \leftarrow u + Dh - z$$

**end for**

---

208 **TODO: Arash: I explained it above. They are algorithm parameters.**

209 Clearly, (3) has this form necessary for using this algorithm. To perform the steps in (6), we need to  
210 evaluate  $\text{prox}_{\mu f}$  and  $\text{prox}_{\rho g}$ . Proximal algorithms are feasible only if these proximal operators can  
211 be evaluated efficiently which, as we show next, is the case for our problem.

212 **Theorem 1.** Let  $f(h) = \sum_k h_k + y_k^2 e^{-h_k}$  and  $g(x) = \|x\|_1$ . Then,

$$\begin{aligned} [\text{prox}_{\mu f}(u)]_k &= \mathcal{W}\left(\frac{y_k^2}{\mu} \exp\left(\frac{1-\mu u_k}{\mu}\right)\right) + \frac{1-\mu u_k}{\mu}, \\ \text{prox}_{\rho g}(u) &= S_{\rho\lambda}(u) \end{aligned}$$

213 where  $\mathcal{W}(\cdot)$  is the Lambert function [5],  $[S_\alpha(u)]_k = \text{sign}(u_k)(|u_k| - \alpha_k)_+$  and  $(v)_+ = v \vee 0$ .

214 *Proof.* If  $f(x) = \sum_k f_k(x_k)$  then  $[\text{prox}_{\mu f}(x)]_k = \text{prox}_{\mu f_k}(u_k)$ . So  $[\text{prox}_{\mu f}(u)]_k =$   
215  $\min_{x_k} \mu(x_k + y_k^2 e^{-x_k}) + \frac{1}{2}(x_k - u_k)^2$ . Setting the derivative to 0 and solving for  $u_k$  gives the  
216 result. Similarly,  $[\text{prox}_{\rho g}(u)]_\ell = \rho\lambda_\ell|z_\ell| + 1/2(z_\ell - u_\ell)^2$ . This is not differentiable, but the solution  
217 must satisfy  $\rho \cdot \lambda_\ell \cdot \partial(|z_\ell|) = u_\ell - z_\ell$  where  $\partial(|z_\ell|)$  is the sub-differential of  $|z_\ell|$ . The solution is  
218 the soft-thresholding operator  $S_{\rho\lambda_\ell}(u_\ell)$ .  $\square$

## 219 4 Empirical evaluation

220 In this section, we examine both simulated and real spatio-temporal climate data. All the computations  
221 were performed on a Linux machine with four 3.20GHz Intel i5-3470 cores.

### 222 4.1 Simulations

223 **TODO: Can we add some type of performance measure? What if we fit 2 marginal models, spatial**  
224 **only and temporal only. Plus maybe a marginal GARCH?**

225 We generate observations at all time steps and all locations from independent Gaussian random  
226 variables with zero mean. However, the variance of these random variables follows a smoothly  
227 varying function in time and space

$$\sigma^2(t, r, c) = \sum_{s=1}^S W_s(t) \cdot \exp\left(\frac{(r - r_s)^2 + (c - c_s)^2}{2\sigma_s^2}\right); \quad W_s(t) = \alpha_s \cdot t + \exp(\sin(2\pi\omega_s t + \phi_s)).$$

228 In words, the variance at each time and location is computed as the weighted sum of  $S$  bell-shaped  
229 functions where the weights are time-varying, consist of a linear trend  $\alpha_s \cdot t$  and a periodic term  
230  $\beta_s \cdot \sin(2\pi\omega_s t + \phi_s)$ . The bell-shaped functions impose the spatial smoothness, and the linear trend  
231 and the periodic terms enforce the temporal smoothness similar to the seasonal component in the  
232 real climate data. We simulated the data on a 5 by 7 grid and for 780 time steps with  $S = 4$ . The  
233 parameters of the variance function are shown in Table 1 in Appendix C. For reference, we plot the



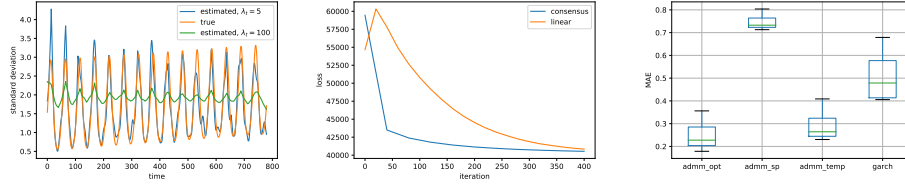


Figure 2: Left: The true (orange) and estimated standard deviation function at the location (0,0). The estimated values are obtained using linearized ADMM with  $\lambda_s = 0.1$  and two values of  $\lambda_t$ :  $\lambda_t = 5$  (blue) and  $\lambda_t = 100$  (green). Middle: Convergence speed of linearized and consensus ADMM. Right: MAE for four models: admm\_opt: the proposed model with optimal values of  $\lambda_t$  and  $\lambda_s$ , admm\_temp: no spatial penalty, admm\_sp: no temporal penalty.

234 variance function for all locations at  $t = 25$  and  $t = 45$  in as well as the variance across time at  $(0, 0)$   
 235 in 4 in Appendix C.

236 We estimated the linearized ADMM for all combinations of values of  $\lambda_t$  and  $\lambda_s$  from the sets  
 237  $\lambda_t \in \{0, 1, 5, 10, 50, 100\}$  and  $\lambda_s \in \{0, 0.05, 0.1, 0.2, 0.3\}$ . For each pair, we then compute the  
 238 mean absolute error (MAE) between the estimated variance and the true variance at all locations and  
 239 all time steps. For  $\lambda_t = 5$  and  $\lambda_s = 0.1$  MAE was minimized. The left panel of 2 shows the true and  
 240 the estimated standard deviation at location (0,0) using  $\lambda_s = 0.1$  and  $\lambda_t = 5$  (blue) and  $\lambda_t = 100$   
 241 (green). As we can see, larger than optimal value of  $\lambda_t$  leads to estimated values which are “too  
 242 smooth”.

243 The middle panel of 2 shows the convergence of Algorithms 1 and 2. Each iteration of the linearized  
 244 algorithm takes 0.01 seconds on average while each iteration of the consensus ADMM takes about  
 245 20 seconds.

246 To further examine the performance of the proposed model, we next compare it to three models: a  
 247 model which does not consider the spatial smoothness and so is equivalent to fitting the model in  
 248 Section 2.1 to each time-series separately, a model which does not consider the temporal smoothness,  
 249 and a GARCH(1,1) model. We simulated 100 datasets using the method explained above with  
 250  $\sigma_s \sim \text{unif}(4, 7)$ . The right panel of 2 shows the boxplot of MAE for these models. Interestingly, the  
 251 proposed model with optimal parameters outperforms GARCH(1,1) in estimating the true value of  
 252 the variance.

253 **TODO: These data are pretty small. Is it possible to do the PDIP?**

254 **TODO: Arash: we can, but why? it will be very slow.**

## 255 4.2 Data analysis

256 Algorithm 1 is appropriate only if we parallelize it over multiple machines, and it is significantly  
 257 slower on our simulated data, so we do not pursue it further here. All the results reported in this  
 258 section are obtained using Algorithm 2. We applied this algorithm to the northern hemisphere of the  
 259 ERA-20C dataset available from the <https://www.ecmwf.int>. The data are the 2 meter temperature  
 260 measured daily at 12 p.m from January 1, 1960 to December 24, 2010.

261 In Appendix D, we investigate some properties of the time-series of different locations on earth. We  
 262 also explain how each time-series is detrended using  $\ell_1$ -trend filtering method explained in Section 2.  
 263 6 shows a time-series after detrending using this method. The variance of this time-series have a  
 264 cyclic behavior. The cycles are not regular and their amplitude and frequency change. In addition,  
 265 the time-series of other locations show different patterns. These observations motivate the need to  
 266 develop a non-parametric framework for the problem at hand. In this figure, the estimate SD obtained  
 267 from the method of Section 2.1 is also shown. Since the estimated SD captures the periodic behavior  
 268 of volatility, it is hard to see the trend in volatility based on these estimated values. Therefore, we  
 269 compute the annual average of these estimates. However, as this figure shows, the annual trend is not  
 270 smooth. This is because in the optimization problem (2), the smoothness of the annual trend is not  
 271 encouraged. Therefore, in Appendix D we propose a simple method to encourage the smoothness of



the annual average trend. The estimated SDs using this method is shown in the right panel of 6. The annual average of the estimated SDs shows a linear trend with a positive slope.

**Convergence** We used the following rule to determine when to stop the optimization: the optimization was stopped if the value of the loss did not improve by at least 0.1% in 1000 trials. Our experiments showed that the convergence speed depends on the value of  $\lambda_t$  and  $\lambda_s$ . Also, if we use the solution obtained for smaller values of these parameters as the initial value for the larger values (*warm start*), the converges speed improves.

**Model selection** One common method for choosing the penalty parameters in the Lasso problems is to find the solution for a range of the values of these parameters and then choose the values which minimize a model selection criterion. However, such analyses needs the computation of the degrees of freedom (df). Several previous work have investigated the df in generalized lasso problems [9, 24, 30]. However, all these studies have considered the linear regression problem and, to the best of our knowledge, the problem of computing the df for generalized lasso with general objective function has not been considered yet.

Another approach is to choose the set of values which minimize an estimate of the expected prediction error obtained by k-fold cross-validation [20]. Although this method is applicable for our problem, it needs k times more computation.

In this paper, we use a heuristic method for choosing  $\lambda_t$  and  $\lambda_s$ : we compute the optimal solution for a range of values of these parameters and choose the values which minimize  $\mathcal{L}(\lambda_t, \lambda_s) = -l(y|h) + \sum \|D_{total}h\|$ . This objective is a compromise between the negative log likelihood ( $-l(y|h)$ ) and the complexity of the solution ( $\sum \|D_{total}h\|$ ). For smoother solutions the value of  $\sum \|D_{total}h\|$  will be smaller but with the cost of larger  $-l(y|h)$ .

We computed the optimal solution for all the combinations of the following sets of values:  $\lambda_t \in \{0, 2, 4, 8, 10, 15, 200, 1000\}$ ,  $\lambda_s \in \{0, .1, .5, 2, 5, 10\}$ . The best combination was  $\lambda_t = 4$  and  $\lambda_s = 2$ . All the analyses in the next section are performed on the solution for these values.

**Analysis of trend of temperature volatility** The top row of 3 shows the detrended data, the estimated standard deviation and the yearly average of these estimates for two cities in the US: Bloomington (left) and San Diego (right). The estimated SD captures the periodic behavior in the variance of the time-series. In addition, the number of linear segments changes adaptively in each time window depending on how fast the variance is changing.

The yearly average of the estimated SD captures the trend in the temperature volatility. For example, we can see that in Bloomington, there is a small positive trend. To determine how the volatility has changed in each location, we subtract the average of the estimated variance in 1992 from the average in the following years and compute their sum. The value of this change in the variance in each location is depicted in the right panel of 3. The left panel of this figure, shows the average estimated variance in each location. Since the optimal value of the spatial penalty is rather large ( $\lambda_s = 2$ ) the estimated variance is spatially very smooth.

It is interesting to note that the trend in volatility is almost zero over the oceans. The most positive trend can be observed in Asia and particularly in south-east Asia.

The bottom panel of 3 shows the histogram of change in the estimated SD across the northern hemisphere. As we can see, the SD in most locations on the northern hemisphere had a negative trend in this time period.

## 5 Discussion

In this paper, we proposed a new method for estimating the variance of spatio-temporal data. The main idea is to cast this problem as a constrained optimization problem where the constraints enforce smooth changes in the variance for neighboring points in time and space. In particular, the solution is piecewise linear in time and piecewise constant in space. The resulting optimization is in the form of a generalized LASSO problem with high-dimension, and so applying the PDIP method directly is infeasible. We therefore developed two ADMM-based algorithms to solve this problem: the consensus ADMM and linearized ADMM.

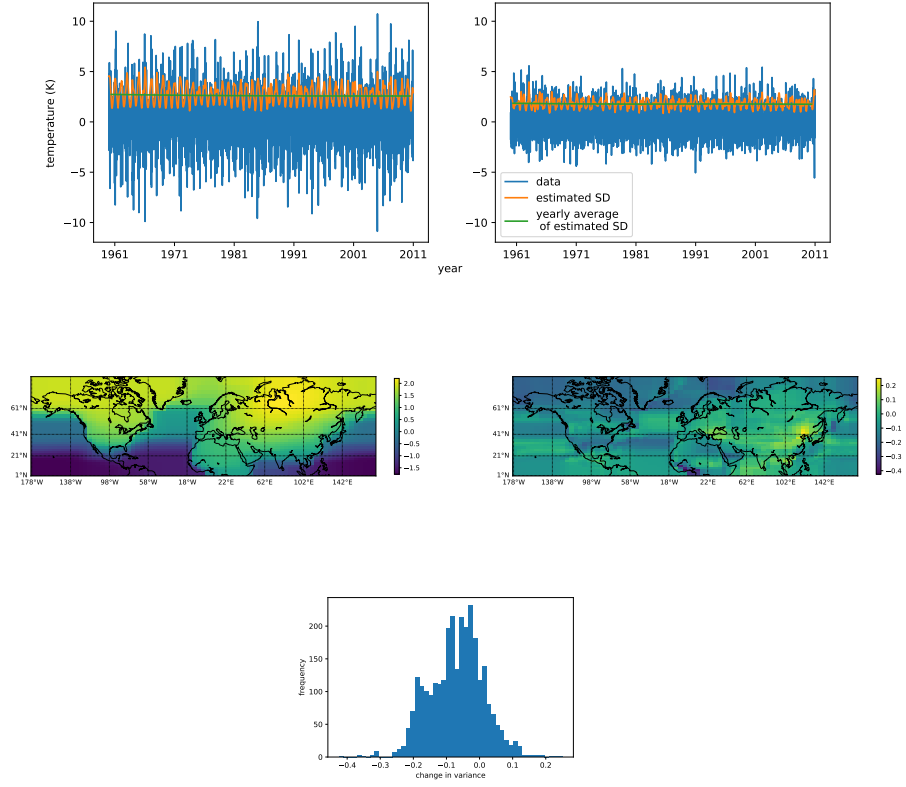


Figure 3: Top row: Detrended data and the estimated SD for Bloomington (left) and San Diego (right). Middle row: the average of the estimated variance over the northern hemisphere (left) and the change in the variance from 1961 to 2011 (right). Bottom: the histogram of change in estimated SD.

The consensus ADMM algorithm converges in few hundreds of iterations but each iteration takes much longer than the linearized ADMM algorithm. The appealing feature of the consensus ADMM algorithm is that if it is parallelized on enough number of machines the computation time per iteration remains constant as the problem size increases. The linearized ADMM algorithm, on the other hand converges in few thousands of iterations but each iteration is performed in split second. However, since the algorithm converges in many iterations it is not very appropriate for parallelization. The reason is that after each iteration the solution computed in each machine should be broadcast to the master machine and this operation takes some time which depends on the speed of the network connecting the slave machines to the master. A direction for future research would be to combine these two algorithms in the following way: the problem should be split into the sub-problems (as in the consensus ADMM) but each sub-problem can be solved using linearized ADMM.

We applied the linearized ADMM algorithm to the surface temperature data on a grid over the united states, for years 1992-2002. The results showed that in many locations the variance of the temperature has increased about 1 unit in 10 years.

The goal of this paper, however, is not to make any conclusions about the trend in the variance because we solved the problem only for a grid over the united states and for 10 years of the data. A thorough analysis, needs the full solution over the globe and for a longer time period. The goal of the paper, was to propose the idea of estimating the trend in variance of spatio-temporal signals using generalized lasso and to investigate the algorithms for solving the resulting optimization problem.

## 6 Appendix A

In this appendix we provide more details on how to solve the optimization problem 2 using PDIP. The objective function is convex but not differentiable. Therefore, to be able to use PDIP we first

344 need to derive the dual of this problem. We note that this is a generalized LASSO problem [21]. The  
 345 dual of a generalized LASSO with the objective  $f(x) + \lambda \|Dx\|_1$  is:

$$\min_{\nu} f^*(-D^\top \nu) \quad \text{s.t.} \quad \|\nu\|_\infty \leq \lambda$$

346 where  $f^*(\cdot)$  is the Fenchel conjugate of  $f$ :  $f^*(u) = \max_x u^\top x - f(x)$ . It is simple to show that

$$f^*(u) = \sum_t (u_t - 1) \log \frac{y_t^2}{1 - u_t} + u_t - 1.$$

347 Each iteration of PDIP involves computing a search direction by taking a Newton step for the system  
 348 of nonlinear equations  $r_w(v, \mu_1, \mu_2) = 0$ , where  $w > 0$  is a parameter and

$$r_w(v, \mu_1, \mu_2) := \begin{bmatrix} r_{dual} \\ r_{cent} \end{bmatrix} = \begin{bmatrix} \nabla f^*(-D^\top v) + \mu_1 - \mu_2 \\ -\mu_1(v - \lambda \mathbf{1}) + \mu_2(v + \lambda \mathbf{1}) - w^{-1} \mathbf{1} \end{bmatrix}$$

349 for  $w > 0$ , where  $\mu_1$  and  $\mu_2$  are dual variables for the  $\ell_\infty$  constraint. Let  $A = [\nabla r_{dual}^\top, \nabla r_{cent}^\top]^\top$ .  
 350 The newton step takes the following form

$$r_w(v, \mu_1, \mu_2) + A \begin{bmatrix} \nabla v \\ \nabla \mu_1 \\ \nabla \mu_2 \end{bmatrix} = 0$$

351 We have:

$$A = \begin{bmatrix} \nabla^2 f^*(-D^\top v) & I & -I \\ -\text{diag}(\mu_1) \mathbf{1} & -v + \lambda \mathbf{1} & \mathbf{0} \\ \text{diag}(\mu_2) \mathbf{1} & v + \lambda \mathbf{1} & \mathbf{0} \end{bmatrix}$$

352 Therefore, to perform the Newton step we need to compute  $\nabla f^*(-D^\top v)$  and  $\nabla^2 f^*(-D^\top v)$ . It is  
 353 straightforward to show that

$$\begin{aligned} \nabla f^*(-D^\top v) &= -\nabla_u f^*(u) D^\top, \quad u = -D^\top v, \quad (\nabla_u f^*(u))_j = \log \left( \frac{y_j^2}{1 - u_j} \right) \\ \nabla^2 f^*(-D^\top v) &= D \nabla_u^2 f^*(u) D^\top, \quad (\nabla_u^2 f^*(u))_j = \text{diag} \left( \frac{1}{1 - u_j} \right) \end{aligned}$$

## 354 7 Appendix B

355 **TODO: put this in nips appendix format**

356 In this Appendix we give more details on performing the x-update step in Equation 5. We need to  
 357 solve the following optimization problem:

$$\hat{x} := \underset{x}{\operatorname{argmin}} \left( \sum_{j=1}^{n_b} (x_j + y_j^2 e^{-x_j}) + (\rho/2) \|x - \tilde{z} + u\|_2^2 + \Lambda^\top |Dx| \right)$$

358 where  $n_b$  is the number of local variables in each sub-cube in 1, and for ease of notation we have  
 359 dropped the subscript  $i$  and superscript  $m$ . Let  $f(x) = \sum_{j=1}^{n_b} (x_j + y_j^2 e^{-x_j}) + (\rho/2) \|x - \tilde{z} + u\|_2^2$ .  
 360 As it was explained in Section 2.1, the dual of this optimization problem is:  $\min_{\nu} f^*(-D^\top \nu)$  with  
 361 the constraints  $|\nu_k| \leq \Lambda_k$ . So to use PDIP we first need to compute the conjugate function  $f^*(\cdot)$ . We  
 362 have:

$$\begin{aligned}
f^*(\xi) &= \max_x \xi^\top x - f(x) \\
&= \max_x \sum_{j=1}^{n_b} (\xi_j x_j - x_j - y_j^2 e^{-x_j} - (\rho/2)(x_j - \tilde{z}_j + u_j))
\end{aligned}$$

363 Setting the derivative of the terms inside the summation to 0, we obtain:

$$\xi_j - y_j^2 e^{-x_j^*} - \rho x_j^* + \rho(\tilde{z}_j - u_j) = 0 \quad (7)$$

364 where  $x^*$  is the maximizer in 7. Then, it can be shown that  $x_j^*$  which satisfies (7) can be obtained as  
365 follows:

$$\begin{aligned}
x_j^* &= \mathcal{W}\left(\frac{y_j^2}{\rho} e^{\phi_j}\right) - \phi_j \\
\phi_j &= \frac{1 - \xi_j - \rho(\tilde{z}_j - u_j)}{\rho}
\end{aligned}$$

366 In this equation,  $\mathcal{W}(\cdot)$  is the *Lambert function* [5]. Finally, the conjugate function is:  $f^*(\xi) =$   
367  $\sum_{j=1}^{n_b} (\xi_j x_j^* - x_j^* - y_j^2 e^{-x_j^*} - (\rho/2)(x_j^* - \tilde{z}_j + u_j))$ .

368 To use PDIP, we also need to evaluate  $\nabla f^*$  and  $\nabla^2 f^*$ . First note that  $\frac{\partial \mathcal{W}(q)}{\partial q} = \frac{\mathcal{W}(q)}{q(1+\mathcal{W}(q))}$  and  
369  $\frac{\partial^2 \mathcal{W}(q)}{\partial q^2} = -\frac{\mathcal{W}^2(q)(\mathcal{W}(q)+q)}{q^2(1+\mathcal{W}(q))^3}$ . Using the chain rule we get:

$$\frac{\partial f^*(\xi)}{\partial \xi_j} = x_j^* + \frac{\partial x_j^*}{\partial \xi_j} \left[ \xi_j - 1 + y_j^2 e^{-x_j^*} + \rho(\tilde{z}_j - u_j - x_j^*) \right]$$

370 where we have:

$$\frac{\partial x_j^*}{\partial \xi_j} = \frac{1}{\rho(1 + \mathcal{W}((y_j^2/\rho)e^{-\phi_j}))}$$

371 By some tedious but straightforward computation we can obtain the second derivatives:

$$\begin{aligned}
\frac{\partial^2 f^*(\xi)}{\partial \xi_j^2} &= \frac{\partial x_j^*}{\partial \xi_j} - \rho \frac{\partial^2 x_j^*}{\partial \xi_j^2} \left[ \phi_j + x_j^* - \tilde{z}_j + u_j \right] \\
&\quad + \frac{\partial x_j^*}{\partial \xi_j} \left[ 1 - y_j^2 \frac{\partial x_j^*}{\partial \xi_j} e^{-x_j^*} - \rho \frac{\partial x_j^*}{\partial \xi_j} \right] \\
\frac{\partial^2 x_j^*}{\partial \xi_j^2} &= \frac{\mathcal{W}((y_j^2/\rho)e^{-\phi_j})}{\rho^2(1 + \mathcal{W}((y_j^2/\rho)e^{-\phi_j}))^3}
\end{aligned}$$

372 Having computed the conjugate function and its gradient and Jacobian, now we can use a number  
373 of convex optimization software packages which have an implementation of PDIP to perform the  
374 x-update step inside the ADMM loop. We chose the python API of the `cvxopt` package [1].

## 375 8 Appendix C

376 Table 1 lists the parameters used for simulating data in Section 4.1. 4 shows the variance  
377 function obtained from there parameters at  $t = 25$  (left) and  $t = 45$  (center).

Table 1: Parameters used to simulate data. **TODO: Any ideas to take up less space with this info?**

$s$	$r_s$	$c_s$	$\sigma_s$	$\alpha_s$	$\omega_s$	$\phi_s$
1	0	0	5	0.5	0.121	0
2	0	5	5	0.1	0.121	0
3	3	0	5	-0.5	0.121	$\pi/2$
4	3	5	5	-0.1	0.121	$\pi/2$



Figure 4: Variance function at  $t = 25$  (left) and  $t = 45$  (center). Right: the true (orange) and estimated standard deviation function at the location (0,0). The estimated values are obtained using linearized ADMM with  $\lambda_s = 0.1$  and two values of  $\lambda_t$ :  $\lambda_t = 5$  (blue) and  $\lambda_t = 100$  (green).

## 9 Appendix D

In this appendix we examine some of the properties of the time-series of the temperature in ERA-20C dataset. The goal here is to demonstrate some of the difficulties in modeling the trend in the temperature volatility and motivate our methodology.

5 shows the time-series of the temperature of three cities: Bloomington (USA), San Diego (USA) and Manaus (Brazil). The time-series of Bloomington and San Diego show clear cyclic behavior. However, while it seems (qualitatively) that these cycles can be modeled by a sinusoidal function for Bloomington, the same is not true for San Diego. Also, the amplitude of the cycles changes from some years to others. The time-series of Manaus does not show any regular cyclic behavior. This demonstrates the first difficulty in analyzing the variance of this data: to analyze the variance, we first need to remove the cyclic terms from all time-series. However, there is a lot of variations in the cyclic behavior of the time-series of different locations. In addition, some of these cycles cannot be easily modeled by a parametric function<sup>4</sup>. To overcome these issues, we use a non-parametric approach to remove the cyclic terms from the time-series and de-trend them. This approach, called  $\ell_1$ -trend filtering is explained in Section 2 of the text. We detrended each time-series separately using this method. For each time-series, we found the optimal value of the penalty parameter using  $k$ -fold cross-validation with  $k = 5$ . We used the R package **genlasso** to perform these computations [2].

<sup>4</sup>One might try to model the cycles by the summation of sinusoidal terms with different frequencies. However, for some time-series this may need many terms to be included in the summation to achieve a reasonable level of accuracy. In addition, this model cannot capture the non-stationarity in the cycles.

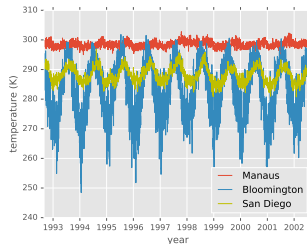


Figure 5: Time-series of the temperature (in Kelvin) of three cities.

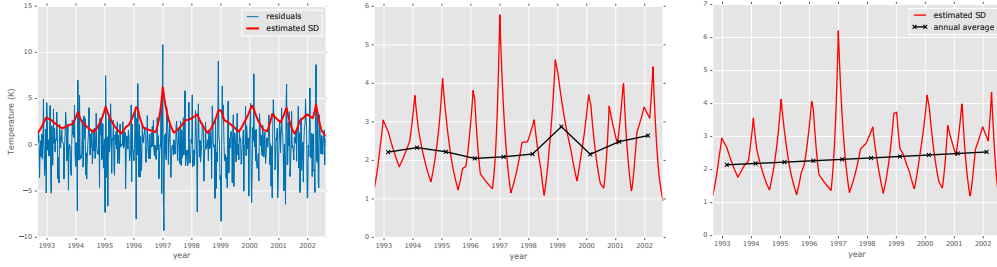


Figure 6: Left: The residuals of the time-series of Bloomington (averaged weekly) and the estimated SD obtained from the method of Section 2.1 (red). Middle: the estimated SDs (red) and their annual average (black) without imposing the long horizon penalty. Right: the same as middle panel but here the long horizon penalty is imposed. See the text for more details.

The blue curve in the left panel of 6 shows the time-series of the temperature of Bloomington after detrending using this method. This figure, reveals another difficulty in estimating the trend of volatility in this data: the variance of this signal, shows cyclic behavior. Also, the cycles are not regular and their amplitude and frequency change. Even if one can describe the behavior of the variance of the time-series at all locations using a single parametric model (for example a variant of the GARCH models [3]), it is not clear how the trend in the variance should be investigated in this framework. These observations motivate the need to develop a non-parametric framework for the problem at hand.

The red curve in the left panel of 6 shows the estimated SD (which is  $\exp(h_t/2)$ ) of the residuals of the time-series of Bloomington obtained from our proposed model. To reduce the number of time-steps we work on the weekly averaged of the data. The curve of the estimated SD captures the periodic variations in the SD of the signal. Just by looking at this curve, it is hard to say if the SD is decreasing or increasing. Therefore, we compute the average of the estimated SD for each year. The estimated SD together with this annual average is shown in the middle panel of 6. As it can be seen, the annual trend is not smooth. This is because in the optimization problem (2), the smoothness of the annual trend is not encouraged. To remedy this, we add the following long horizon penalty to (2):

$$\sum_{i=1}^{N_{year}-2} \left| \sum_{t=1}^{52} h_{t_1} - 2h_{t_2} + h_{t_3} \right| \quad (8)$$

where  $t_1 = 52(i-1) + t$ ,  $t_2 = 52i + t$  and  $t_3 = 52(i+1) + t$ . Also,  $N_{year}$  is the number of years over which we are performing our analysis (here  $N_{year} = 10$ ). Since we are working on the weekly averaged data, each year corresponds to 52 observations. In the matrix form, the penalty (8) adds  $N_{year}$  rows to the matrix  $D$ . The estimated SDs using this penalty matrix is shown in the right panel of 6. The annual average of the estimated SDs shows a linear trend with a positive slope.

## References

- [1] M. S. Andersen, J. Dahl, and L. Vandenberghe. CVXOPT: A Python package for convex optimization, version 1.1. 6. Available at [cvxopt.org](http://cvxopt.org) 54, 2013.
- [2] T. B. Arnold and R. J. Tibshirani. Efficient Implementations of the Generalized Lasso Dual Path Algorithm. *Journal of Computational and Graphical Statistics*, 25(1):1–27, Jan. 2016.
- [3] T. Bollerslev. Generalized autoregressive conditional heteroskedasticity. *Journal of Econometrics*, 31(3): 307–327, Apr. 1986. ISSN 0304-4076.
- [4] S. Boyd, N. Parikh, E. Chu, B. Peleato, and J. Eckstein. Distributed Optimization and Statistical Learning via the Alternating Direction Method of Multipliers. *Foundations and Trends in Machine Learning*, 3(1): 1–122, 2011. ISSN 1935-8237.

- [5] R. M. Corless, G. H. Gonnet, D. E. G. Hare, D. J. Jeffrey, and D. E. Knuth. On the LambertW function. *Advances in Computational Mathematics*, 5(1):329–359, Dec. 1996.
- [6] E. M. Fischer, U. Beyerle, and R. Knutti. Robust spatially aggregated projections of climate extremes. *Nature Climate Change*, 3:1033–1038, 2013. URL <http://dx.doi.org/10.1038/nclimate2051>.
- [7] D. Hallac, Y. Park, S. Boyd, and J. Leskovec. Network inference via the time-varying graphical lasso. In *Proceedings of the 23rd ACM SIGKDD International Conference on Knowledge Discovery and Data Mining*, KDD ’17, pages 205–213, New York, NY, USA, 2017. ACM. doi: 10.1145/3097983.3098037. URL <http://doi.acm.org/10.1145/3097983.3098037>.
- [8] J. Hansen, M. Sato, and R. Ruedy. Perception of climate change. *Proceedings of the National Academy of Sciences*, 109(37), Sept. 2012.
- [9] Q. Hu, P. Zeng, and L. Lin. The dual and degrees of freedom of linearly constrained generalized lasso. *Computational Statistics & Data Analysis*, 86:13–26, June 2015.
- [10] C. Huntingford, P. D. Jones, V. N. Livina, T. M. Lenton, and P. M. Cox. No increase in global temperature variability despite changing regional patterns. *Nature*, 500(7462):327–330, Aug. 2013. ISSN 0028-0836.
- [11] S. Kim, K. Koh, S. Boyd, and D. Gorinevsky.  $\ell_1$  Trend Filtering. *SIAM Review*, 51(2):339–360, May 2009. ISSN 0036-1445. doi: 10.1137/070690274. URL <http://epubs.siam.org/doi/abs/10.1137/070690274>.
- [12] S.-J. Kim, K. Koh, S. Boyd, and D. Gorinevsky.  $\ell_1$  trend filtering. *SIAM Review*, 51(2):339–360, 2009. doi: 10.1137/070690274. URL <https://doi.org/10.1137/070690274>.
- [13] K. Lin, J. L. Sharpnack, A. Rinaldo, and R. J. Tibshirani. A sharp error analysis for the fused lasso, with application to approximate changepoint screening. In I. Guyon, U. V. Luxburg, S. Bengio, H. Wallach, R. Fergus, S. Vishwanathan, and R. Garnett, editors, *Advances in Neural Information Processing Systems 30*, pages 6884–6893. Curran Associates, Inc., 2017. URL <http://papers.nips.cc/paper/7264-a-sharp-error-analysis-for-the-fused-lasso-with-application-to-approximate-changepoint-screening.pdf>.
- [14] N. Parikh and S. Boyd. Proximal Algorithms. *Foundations and Trends® in Optimization*, 1(3):127–239, Jan. 2014.
- [15] A. Ramdas and R. J. Tibshirani. Fast and flexible admm algorithms for trend filtering. *Journal of Computational and Graphical Statistics*, 25(3):839–858, 2016.
- [16] A. Rhines and P. Huybers. Frequent summer temperature extremes reflect changes in the mean, not the variance. *Proceedings of the National Academy of Sciences*, 110(7):E546–E546, Feb. 2013.
- [17] V. Sadhanala, Y.-X. Wang, J. L. Sharpnack, and R. J. Tibshirani. Higher-order total variation classes on grids: Minimax theory and trend filtering methods. In I. Guyon, U. V. Luxburg, S. Bengio, H. Wallach, R. Fergus, S. Vishwanathan, and R. Garnett, editors, *Advances in Neural Information Processing Systems 30*, pages 5800–5810. Curran Associates, Inc., 2017. URL <http://papers.nips.cc/paper/7162-higher-order-total-variation-classes-on-grids-minimax-theory-and-trend-filtering-methods.pdf>.
- [18] J. A. Screen. Arctic amplification decreases temperature variance in northern mid- to high-latitudes. *Nature Climate Change*, 4:577–582, 2014. URL <http://dx.doi.org/10.1038/nclimate2268>.
- [19] P. W. Staten, B. H. Kahn, M. M. Schreier, and A. K. Heidinger. Subpixel characterization of HIRS spectral radiances using cloud properties from AVHRR. *Journal of Atmospheric and Oceanic Technology*, 33(7): 1519–1538, 2016. doi: 10.1175/JTECH-D-15-0187.1.
- [20] R. Tibshirani. Regression Shrinkage and Selection via the Lasso. *Journal of the Royal Statistical Society. Series B (Methodological)*, 58(1):267–288, 1996.
- [21] R. J. Tibshirani. *The Solution Path of the Generalized Lasso*. PhD Thesis, Stanford University, 2011.
- [22] R. J. Tibshirani. Adaptive piecewise polynomial estimation via trend filtering. *Annals of Statistics*, 42: 285–323, 2014. URL <http://www.stat.cmu.edu/~ryantibs/papers/trendfilter.pdf>.
- [23] R. J. Tibshirani and J. Taylor. The solution path of the generalized lasso. *Annals of Statistics*, 39(3): 1335–1371, 2011.



- 475 [24] R. J. Tibshirani and J. Taylor. Degrees of freedom in lasso problems. *The Annals of Statistics*, 40(2):  
476 1198–1232, 2012.
- 477 [25] K. E. Trenberth, Y. Zhang, J. T. Fasullo, and S. Taguchi. Climate variability and relationships between  
478 top-of-atmosphere radiation and temperatures on earth. *Journal of Geophysical Research: Atmospheres*,  
479 120(9):3642–3659, 2014. doi: 10.1002/2014JD022887.
- 480 [26] S. M. Uppala, P. W. K  llberg, A. J. Simmons, U. Andrae, and e. al. The ERA-40 re-analysis. *Quarterly*  
481 *Journal of the Royal Meteorological Society*, 131(612):2961–3012, Oct. 2005.
- 482 [27] D. A. Vasseur, J. P. DeLong, B. Gilbert, H. S. Greig, C. D. G. Harley, K. S. McCann, V. Savage, T. D.  
483 Tunney, and M. I. O’Connor. Increased temperature variation poses a greater risk to species than climate  
484 warming. *Proceedings of the Royal Society of London B: Biological Sciences*, 281(1779), 2014. doi:  
485 10.1098/rspb.2013.2612.
- 486 [28] Y.-X. Wang, J. Sharpnack, A. J. Smola, and R. J. Tibshirani. Trend filtering on graphs. *Journal of Machine*  
487 *Learning Research*, 17(105):1–41, 2016. URL <http://jmlr.org/papers/v17/15-147.html>.
- 488 [29] Y.-X. Wang, J. Sharpnack, A. J. Smola, and R. J. Tibshirani. Trend Filtering on Graphs. *Journal of Machine*  
489 *Learning Research*, 17(105):1–41, 2016. URL <http://jmlr.org/papers/v17/15-147.html>.
- 490 [30] P. Zeng, Q. Hu, and X. Li. Geometry and Degrees of Freedom of Linearly Constrained Generalized Lasso.  
491 *Scandinavian Journal of Statistics*, 44(4):989–1008, Nov. 2017. ISSN 0303-6898.